



Contents lists available at ScienceDirect

Arabian Journal of Chemistry

journal homepage: www.ksu.edu.sa

A pine leaf form acrylic resin coated coomassie brilliant blue g250-*nido*-carborane fluorescent complex strategy for tumor cell imaging

Jianpeng Hu^{a,1}, Haixia Gu^{a,1}, Zhipeng Xu^a, Yuanye Wan^a, Guofan Jin^{b,*}

^a Jiangsu University, Affiliated Peoples Hospital, Zhenjiang 212001, Jiangsu, PR China

^b School of Pharmacy, Jiangsu University, Zhenjiang 212013, PR China

ARTICLE INFO

Keywords:

Nido-carborane
Coomassie brilliant blue G250
Zwitterion complex
Acrylic resin
Tumor cell imaging

ABSTRACT

Four distinct fluorescence complexes were prepared using a one-pot method: The L100-55-fluorescent complex (LFC), EPO-fluorescent complex (EFC), RS-fluorescent complex (SFC), and RL-fluorescent complex (RFC), respectively. The water solubility, selectivity, and visualization of the carborane have drawn a lot of attention. The carborane's low solubility is resolved, and Coomassie Brilliant Blue (CBB) G250-*nido*-carborane's biocompatibility is enhanced. The LFC complex was observed to scaly, branch and spread in (Scanning Electron Microscope) SEM and (Transmission Electron Microscope) TEM, like the pine leaves tightly covering the zwitterion complex. It was discovered that the fluorescent complex of LFC has strong selectivity and can accurately infiltrate tumor cells by imaging of tumor cells in vitro, suggesting that LFC has good biocompatibility. Human prostate cancer cells (PC3), human cervical cancer cells (HeLa) and Human normal liver cells (LO2) were evaluated under ten various concentration circumstances in the (Cell Counting Kit-8) CCK8 experiment. The proliferation impact was found to be 57.29% and 59.41%, respectively. shown the complex's strong anti-tumor action and little cytotoxicity. The design not only provides an excellent visual fluorescence targeting effect, but it also addresses the issue of *nido*-carborane-coomassie brilliant blue G250's bioavailability.

1. Introduction

With an icosahedron and 26 delocalized electrons, carborane ($C_2H_2B_{10}H_{10}$) is a boron molecule that is comparable in size to a benzene ring (Fig. 1) (Shao et al., 2021, Zhao et al., 2021, Lu et al., 2023). As a result, they and benzene have many characteristics in common, including aromaticity and superior thermal and chemical stability. However, the unique feature of carborane's chemical structure—ten boron atoms' vacant electron orbitals and a massive steric hindrance skeleton that resembles C60—makes it extremely hydrophobic (Hayakawa et al., 2023, Zhang et al., 2023). In addition to playing a stable role, the change of carborane's chemical structure enhances its water solubility and biocompatibility, allowing for a wider and more practical use of the substance in the field of biomedicine. For example: in organic optical materials used as organic light emitting diode (OLED), they are used as functional modules in supramolecular and nanomaterials and carborane compounds are used as high boron content drugs in boron neutron capture therapy (BNCT) for cancer treatment (Sforzi et al., 2023, Shi et al., 2023). In order to broaden its application, effective

acquisition of functionalized derivatives of carborane has become a major research path in the field of carborane chemistry (Beerwerth and Böhmer, 2023, Phung et al., 2023, Zimina et al., 2023).

A water-soluble organic reagent for protein staining and binding analysis is Coomassie Brilliant Blue (CBB) G-250 (Fig. 1). Red in the free form, Coomassie brilliant Blue G-250 has a maximum light absorption wavelength of 488 nm (Ecer et al., 2023, Nagata et al., 2023, Bai et al., 2023, Hasani et al., 2021). When paired with proteins, it becomes cyan, and protein-coupled pigments absorb the most light. It is possible to quantify protein using the light absorption value, which is correlated with the amount of protein (Valibeknejad et al 2023, Wu et al., 2023, Wang et al., 2023). After the protein binds to CBB-G-250, the reaction rapidly reaches equilibrium and is conjugated, allowing the protein to stay stable at room temperature for an hour. This process takes around two minutes. Bradford developed this procedure in 1976 (Hu et al., 2022, Mohamed et al., 2023, Pariary et al., 2023, Wu et al., 2023). The reagent is very sensitive, straightforward to use, and simple to manufacture. It can be applied to ascertain the protein concentration in micrograms and within the range of 0–1000 $\mu\text{g/mL}$. It is a regularly used

* Corresponding author.

E-mail address: organicboron@ujs.edu.cn (G. Jin).

¹ Jianpeng Hu and Haixia Gu contribute equally to this work.

<https://doi.org/10.1016/j.arabjc.2023.105511>

Received 18 July 2023; Accepted 29 November 2023

Available online 1 December 2023

1878-5352/© 2023 The Author(s). Published by Elsevier B.V. on behalf of King Saud University. This is an open access article under the CC BY-NC-ND license (<http://creativecommons.org/licenses/by-nc-nd/4.0/>).

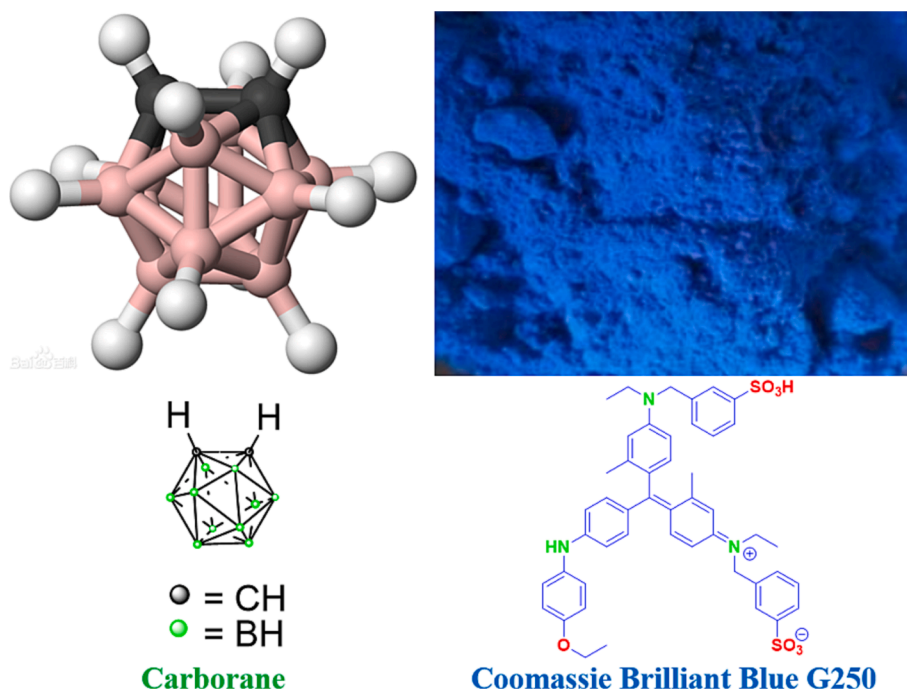
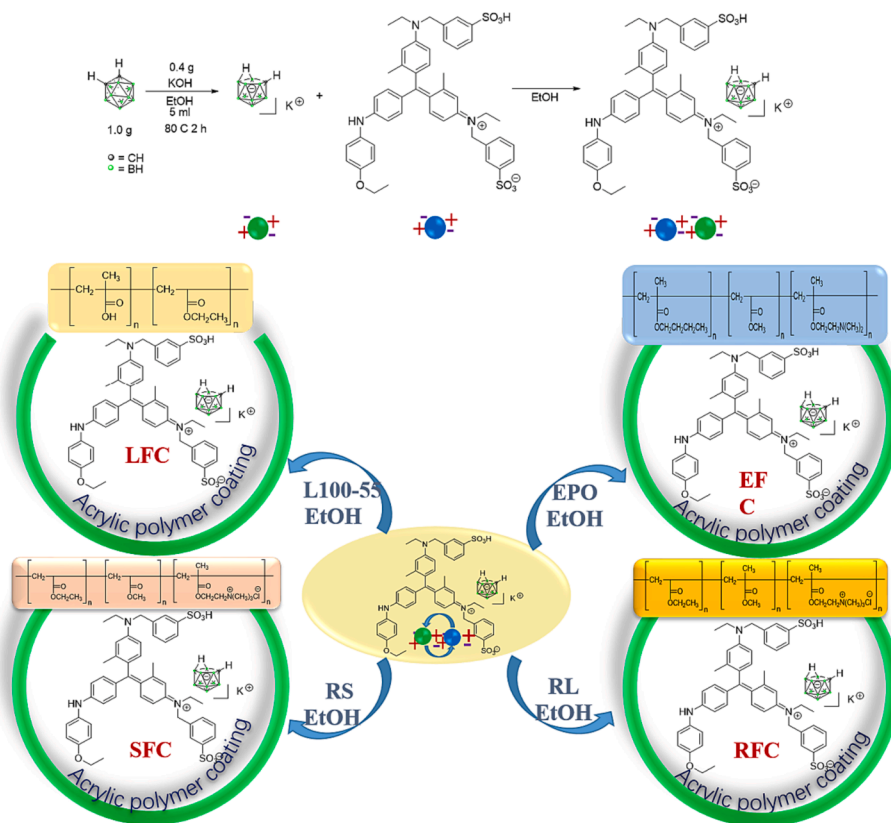


Fig. 1. Carborane and Coomassie Brilliant Blue G250 structures. (For interpretation of the references to colour in this figure legend, the reader is referred to the web version of this article.)



fast micromethod for the detection of protein content (Wang et al., 2021, Shao et al., 2022).

EPO, L100-55, RS, and RL are the four forms of Eudragit that are most commonly utilized as pharmaceutical excipients. It is an important

ingredient and basic raw material used in pharmaceutical preparations; research and production of these products depend on it. It also strongly correlates with its diversity, quality, and dependability, as well as with reducing side effects and increasing medication efficacy (Xu et al.,

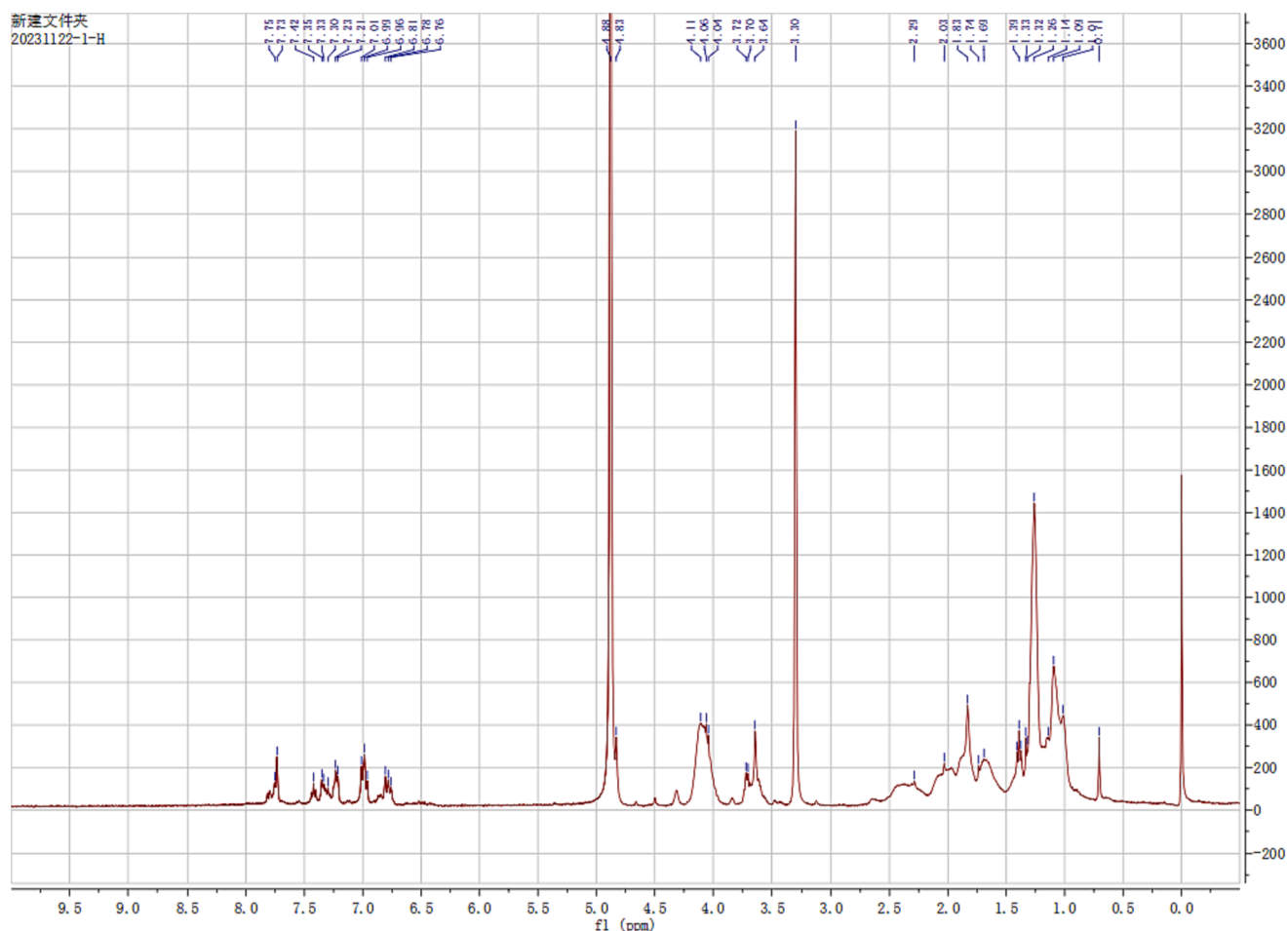


Fig. 2. ^1H NMR spectra of LFC (CD_3OD).

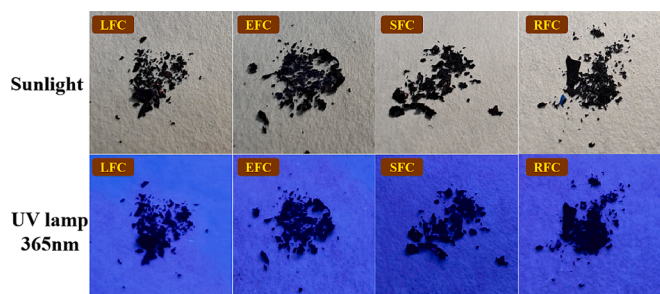


Fig. 3. Comparison of four fluorescent complexes under sunlight and 356 nm irradiation.

2021). Polymer excipients are extensively utilized in the pharmaceutical industry and comprise a significant portion of the excipients used in medicinal compositions. And also the polymers used in the other domains of treatment and protection of the environments (Asmaa, B et al., 2022, Asmaa, B et al., 2023, Asmaa, B et al., 2022). Its chemical properties are stable, it adapts well to physiological tissues, and it is not broken down by the body when used as a medicinal polymer excipient. Its breakdown products won't induce tissue variation or inflammation because they are non-toxic (Liu et al., 2022, Liu et al., 2022, Lee et al., 2023).

In conjunction with the features of the aforementioned analysis, various forms of acrylic resin (Eudragit) coating were utilized to create anti-tumor fluorescent composite medications with good fluorescence effect, utilizing the high activity of carborane and the protein staining

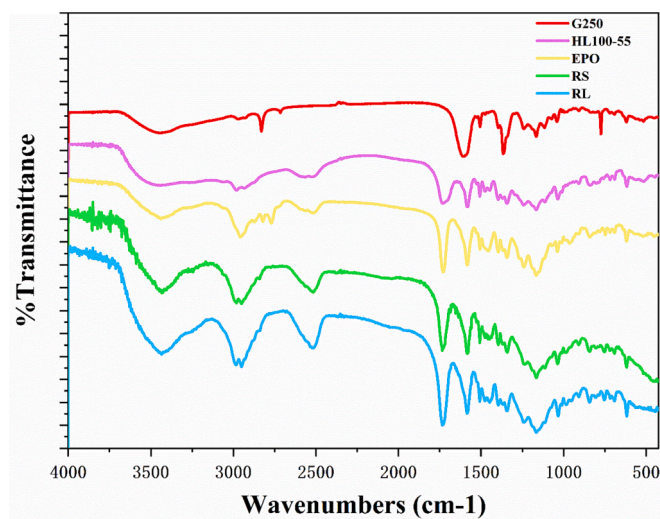


Fig. 4. Infrared spectra of four fluorescent complexes.

ability of CBB-G-250 as a breakthrough.

2. Experiment

2.1. Materials and instruments

All solvents and reagents were purchased commercially and used

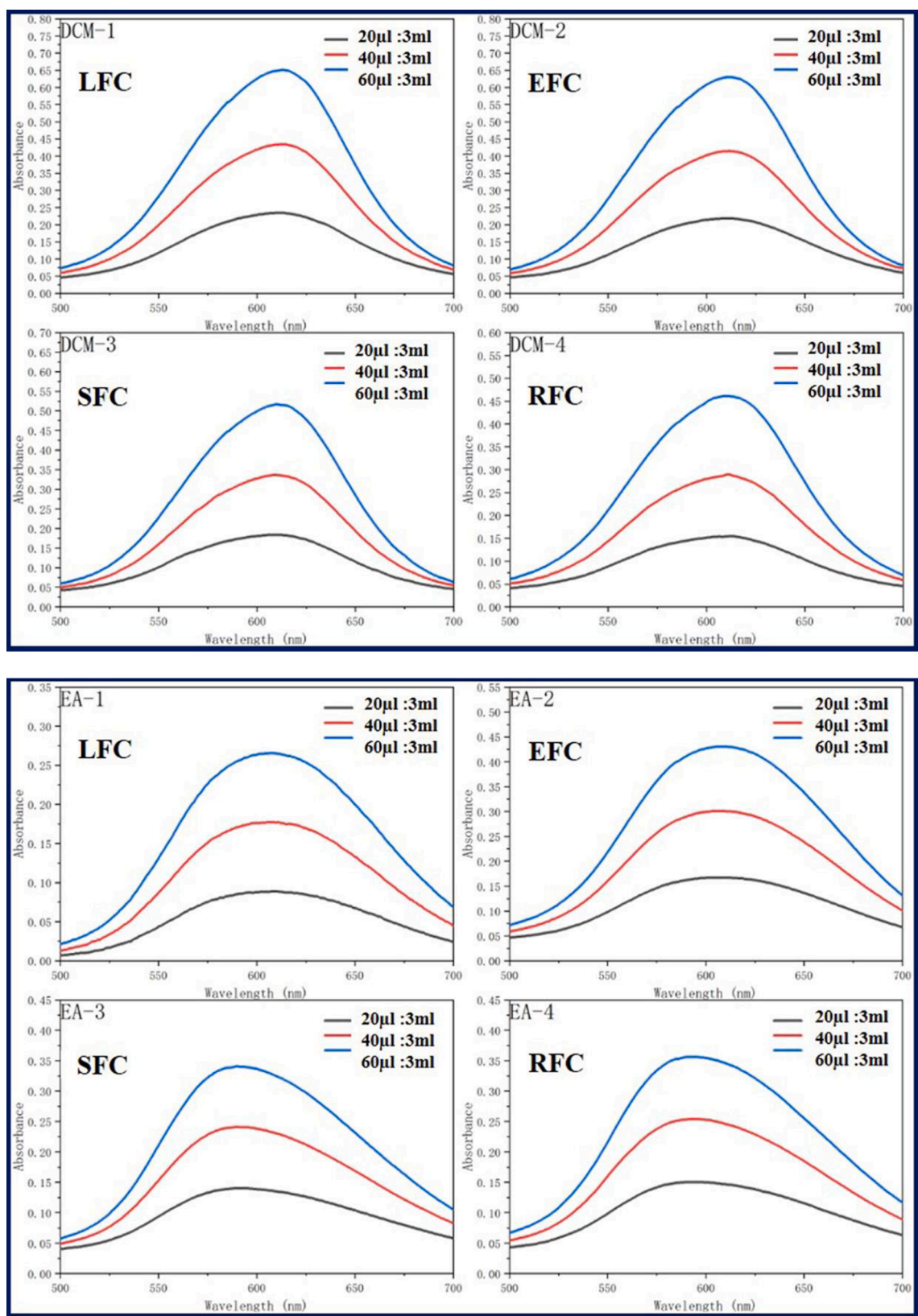


Fig. 5. Ultraviolet absorption of four fluorescent complexes in different solvents and concentrations.

without further purification. The reagents used are carborane (98%, RG: Guaranteed reagent) and coomassie brilliant blue G250 (98%, RG: Guaranteed reagent), which were purchased through commercial

channels such as Titan Technologies. Full-wavelength absorption spectra were recorded using a UV-2550 spectrophotometer. Under excitation at 490 nm, the fluorescence emission spectrum of Shimadzu

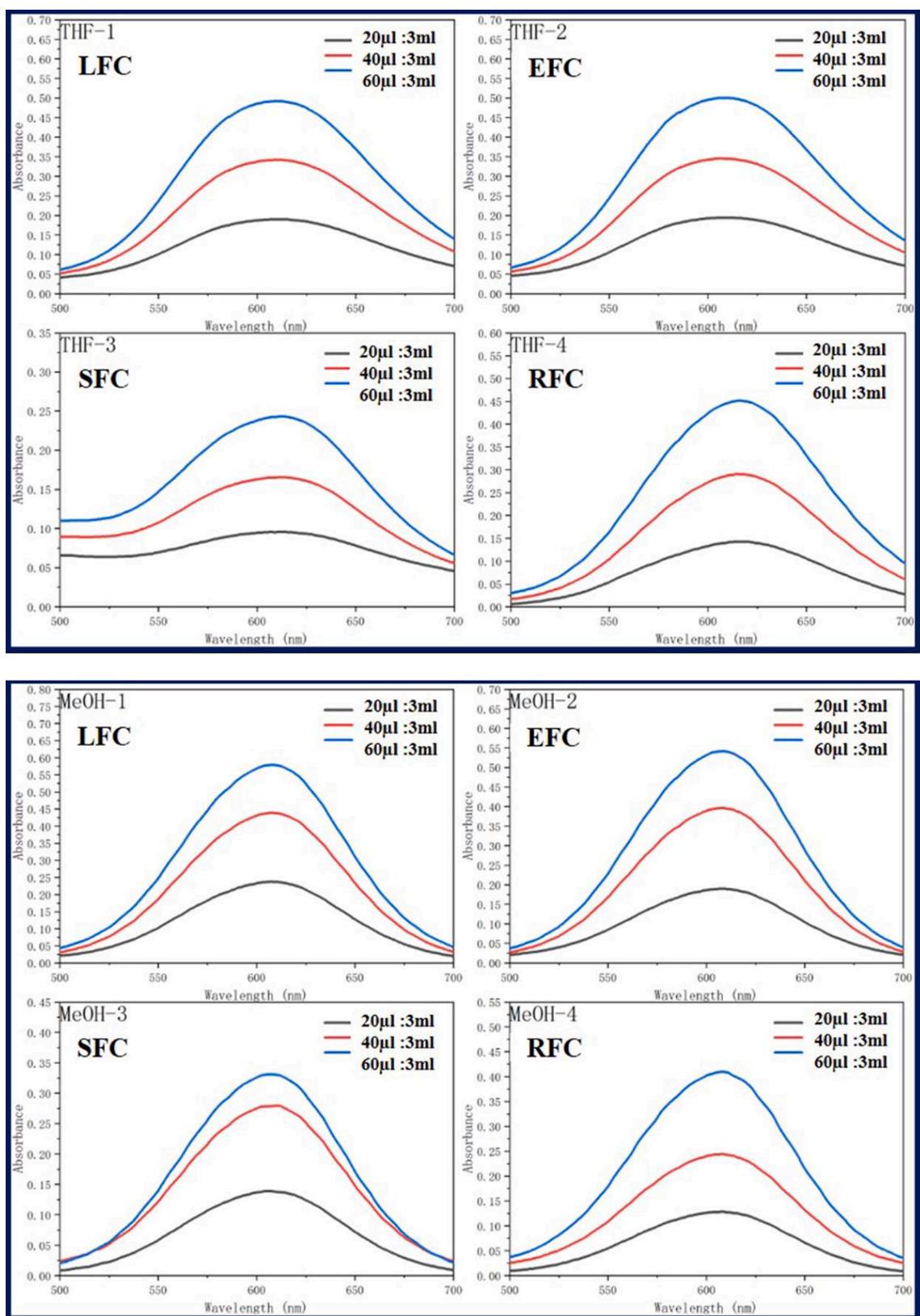


Fig. 5. (continued).

RF-5301pcs spectrophotometer was measured. All optical measurements were performed at room temperature.

2.2. Synthesis

Nido-carborane (20 mg, 0.1 mmol) and CBB-G-250 (100 mg, 0.1 mmol) were dissolved in EtOH (3 mL) at the room temperature stirred

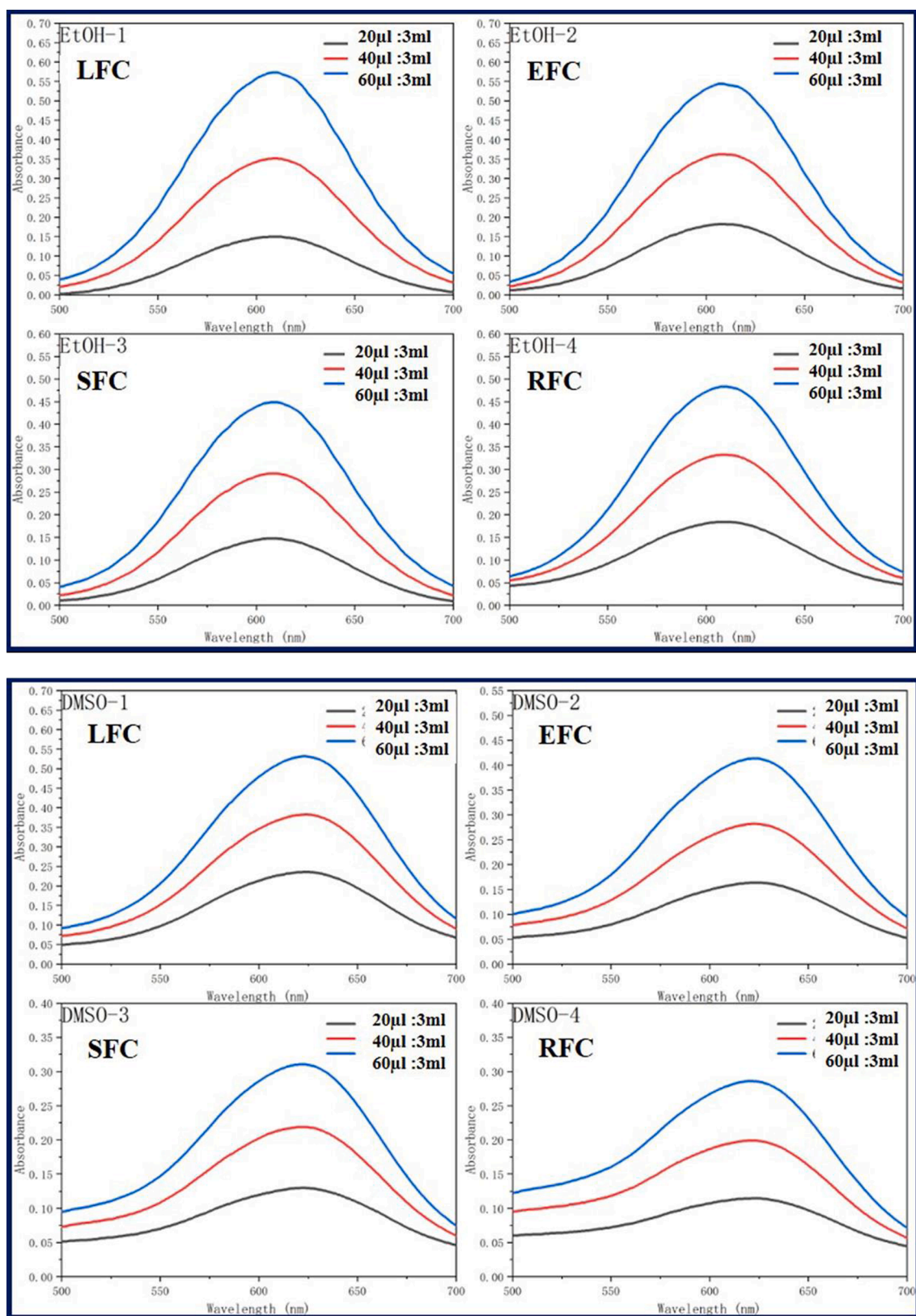


Fig. 5. (continued).

for 1 h. The EtOH was concentrated to afford 120 mg of complex.

Coomassie brilliant blue G250-*nido*-carborane complex 120 mg was reacted with L100-55, EPO, RS and RL = 100 mg (Complex: Eudragit = 1.2:1.0, Mass ratio calculation), respectively, in ethanol 3 mL for 3 h.

The EtOH was concentrated to afford 40 mg of LRFC.

The EFC, SFC and RFC were obtained by the same method.

Table 1

Ultraviolet absorption of four fluorescent complexes in different solvents at 20 $\mu\text{L}:\text{3mL}$.

Compound	Items	Solvents (20 $\mu\text{L}:\text{3mL}$)					
		DCM	EA	THF	EtOH	MeOH	DMSO
LFC	λ_{abs}	611	605	611	613	608	624
EFC	λ_{abs}	611	605	610	610	609	624
SFC	λ_{abs}	609	593	614	608	606	622
RFC	λ_{abs}	612	593	615	609	608	624

Table-2

Ultraviolet absorption of four fluorescent complexes in different solvents at 40 $\mu\text{L}:\text{3mL}$.

Compound	Items	Solvents (40 $\mu\text{L}:\text{3mL}$)					
		DCM	EA	THF	EtOH	MeOH	DMSO
LFC	λ_{abs}	612	604	611	609	608	623
EFC	λ_{abs}	611	607	610	609	608	624
SFC	λ_{abs}	609	591	611	608	610	622
RFC	λ_{abs}	611	593	615	610	609	623

Table-3

Ultraviolet absorption of four fluorescent complexes in different solvents at 60 $\mu\text{L}:\text{3mL}$.

Compound	Items	Solvents (60 $\mu\text{L}:\text{3mL}$)					
		DCM	EA	THF	EtOH	MeOH	DMSO
LFC	λ_{abs}	613	605	611	609	608	623
EFC	λ_{abs}	612	608	610	608	608	623
SFC	λ_{abs}	610	593	613	609	607	622
RFC	λ_{abs}	609	593	617	609	608	622

Table 4

The proliferation rate of PC3 and Hela cells treated by different concentrations of LFC.

Concentration ($\mu\text{g}/\text{mL}$)	0	3.2	4.8	6.4	8	9.6	11.2	12.8	14.4	16
PC3	100.00	92.07%	77.13%	76.14%	73.52%	71.62%	67.42%	65.56%	63.11%	59.41%
Hela	100.00	88.48%	83.65%	75.56%	71.39%	59.90%	56.76%	60.70%	61.79%	57.29%
LO2	100.00	98.46%	91.86%	90.97%	89.34%	88.87%	83.11%	82.01%	79.43%	69.25%

2.3. Spectroscopic properties

2.3.1. UV spectrum

The 20 mg fluorescent complex was dissolved in methylene chloride (MC), ethyl acetate (EA), methanol (MeOH), ethanol (EtOH), dimethyl sulfoxide (DMSO), and tetrahydrofuran (THF), respectively, to prepare the necessary optimal concentration gradient for future use. Spectral tests of solutions with different concentrations were prepared according to needs and data were recorded. The UV-Vis wavelength range is 400–700 nm. The fluorescence of the complex was obtained at the optical path of 10 mm and the excitation wavelength of 450 nm. The wavelength range of the recorded emission was 400–800 nm.

2.3.2. Scanning electron microscope (SEM) test

First, the sample to be tested is ground, then a small amount of sample is glued to the conductive adhesive, the sample is sprayed with platinum, and finally the sample is placed under the field emission scanning electron microscope for detection.

2.4. Cellular uptake and localization by transmission electron microscope (TEM)

Transmission Electron Microscope (TEM) was performed on a Zeiss Ultra Plus at an accelerating voltage of 15 keV, with an attached Oxford Instruments X-Max 60 mm² SDD X-ray microanalysis system. The ethanol suspended precipitate of the sample was added to a silicon wafer, and the sample was attached to a sample tray with a conductive adhesive, and TEM images were obtained using a scanning at 2.0 μm and 200 nm rulers, respectively. Prior to performing ultrasonic oscillation for ten to thirty minutes, a thin supporting film is applied to the copper net, and the appropriate amount of powder and tetrahydrofuran are added to the small beaker, respectively. A glass capillary tube is used to draw out the homogeneous mixture of powder and tetrahydrofuran after

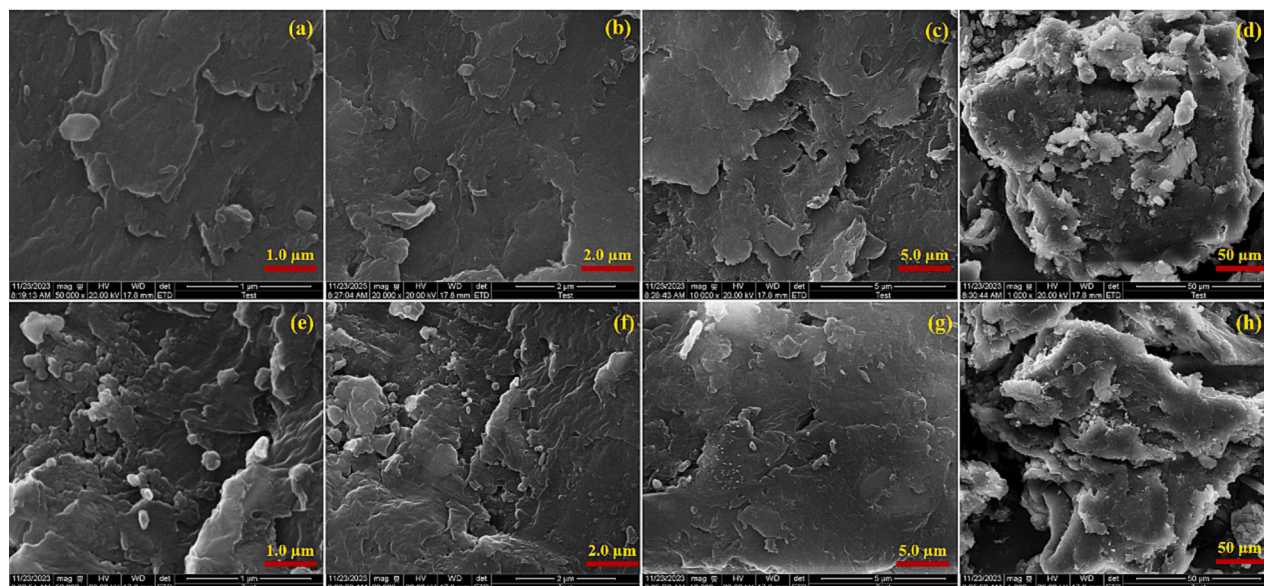


Fig. 6. Scanning electron microscopy diagrams (a), (b), (c), (d), (e), (f), (g), and (h) of fluorescent complex LFC.

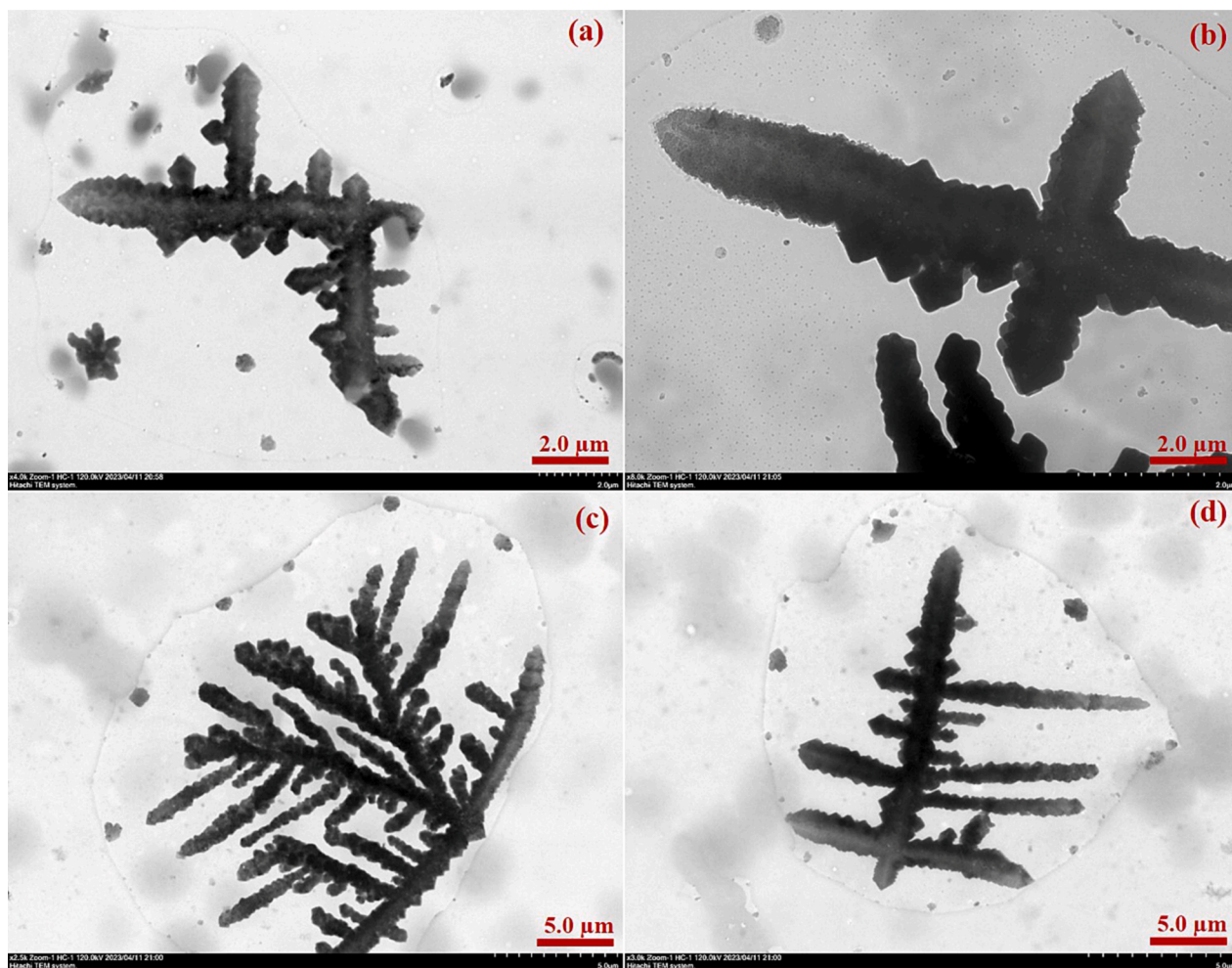


Fig. 7. Transmission electron microscopy diagrams (a), (b), (c) and (d) of fluorescent complex LFC.

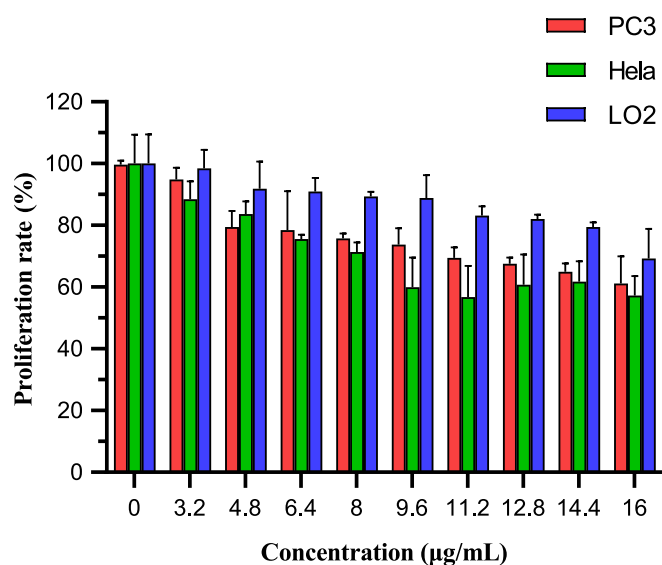


Fig. 8. The proliferation rate of PC3, HeLa and LO2 cells treated by LFC at 10 concentrations (0, 3.2, 4.8, 6.4, 8, 9.6, 11.2, 12.8, 14.4, 16 μg/mL). In the figure, orange represents PC3 cells and green represents HeLa cells. (For interpretation of the references to colour in this figure legend, the reader is referred to the web version of this article.)

three to five minutes. Two to three droplets of the mixture are then placed onto the copper net and allowed to dry. To maximize tetrahydrofuran volatilization, wait longer than 15 min. Lastly, place the sample on the sample table and see it under an electron microscope.

2.5. Cell proliferation toxicity test (CCK8)

Cell pretreatment: Trypsin was used to digest PC3 and HeLa cells in the logarithmic growth phase. The cells were then reorganized into a cell suspension and the concentration was changed. Each group received three wells, with 5000 cells per well injected onto 96-well plates. **Cell dosage treatment:** based on the experimental groups, LFC was added to individual experimental groups at different concentrations (3.2, 4.8, 6.4, 8, 9.6, 11.2, 12.8, 14.4, 16 μg/mL) for a duration of 24 h. Blank control groups were created with an LFC concentration of 0 μg/mL. Following a 24-hour period, extract the cells, fill each well with 10 mL of CCK-8 solution, and let the mixture sit for an hour in the incubator. **Calculating absorbance value:** Measure the absorbance at 450 nm with a microplate reader, store the results, and submit them for analysis. **Calculation of the formula:** $\text{Proliferation\%} = \frac{\text{experimental empty}}{\text{control empty}} * 100\%$. **Inhibition\% = $\frac{\text{experimental control}}{\text{empty control}} * 100\%$.**

2.6. Cell imaging

Trypsin was applied to HeLa cells in the logarithmic growth phase before they were seeded in a 96-well plate with a circular cover,

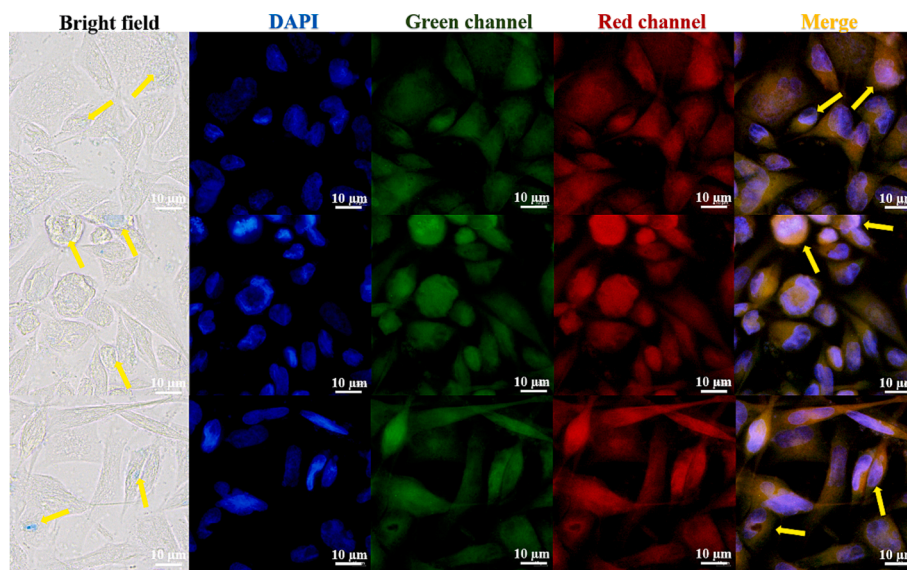


Fig. 9. Fluorescence imaging of LFC fluorescent complexes in different channel HeLa cells.

incubated in an incubator with 5% CO₂, and cultured at 37 °C for 24 h to promote adhesion. To prepare the proper quantities of solution, the prepared polymer LFC stock solutions (20 mg/mL) were made in DMSO, respectively, and then diluted with DMSO. In every sample, the cells in the original culture medium were taken out and replaced with a media containing 20 μg/ml for a whole day. It was then disposed of using PBS, cleaned twice, and fixed for twenty-five minutes with paraformaldehyde. After removing the repair solution with PBS and twice washing the mixture, the solution was treated with anti-fluorescence inactivating scaffolds, incubated in a DAPI dark room for 25 min, and fluorescent images of the cells were taken using a fluorescence microscope.

3. Results and discussion

The continuous method is primarily used in the synthesis design phase to prepare the scheme: First, carborane is treated with strong alkali potassium hydroxide to solve the solubility issue and form small molecules known as zwitterion; second, it undergoes a mixed reaction with CBB-G-250 to form an ionic bond; Lastly, it can combine with various acrylic resin kinds to create polymer aggregation form and an excellent coating effect (Scheme 1). The nuclear magnetic hydrogen (¹H NMR) spectrum shows that CBB-G-250's aromatic ring characteristic peaks lie between 8.0 and 6.5 ppm. Eudragit L100-55 and Coomasil Brilliant Blue G250's branch chain and ethyl or methyl characteristic peaks make up the remaining peaks (Fig. 2). The hue of the four fluorescent compounds produced using the aforementioned preparation techniques was compared at 356 nm and in direct sunshine. The four fluorescent complexes displayed dull black or dark shapes under sunlight (Fig. 3), that were nearly dark at 365 nm.

The four fluorescent compounds covered by the infrared spectrometer were evaluated individually to view their distinctive peak curves. The characteristic absorption peak of CBB-G-250 is located near 1750 cm⁻¹, whereas the characteristic peak of *nidao*-carborane is located about 2500 cm⁻¹. The two chemicals were well confined based on these findings (Fig. 4).

Dichloromethane (MC), dimethylsulfoxide (DMSO), ethylacetate (EA), ethanol (EtOH), methanol (MeOH), and tetrahydrofuran (THF) were used as solvents to analyze the UV spectra of the four fluorescent complexes. The findings demonstrated that, at various solvent concentrations and MC, EtOH, and MeOH, the UV absorbance of the four fluorescent complexes was around 610 nm. The DMSO solvent exhibits

the largest absorption wavelength, whereas EA solvent shows the shortest absorption wavelength. This is due to the influence of the solubility and zwitteric binding of the nested carborane and CBB-G-250 coated with acrylic resin in dimethyl sulfoxide solvent, resulting in a faint red shift. However, because dimethyl sulfoxide has greater solubility and a stronger zwitteric binding action than other solvents, its absorption wavelength is different in those other solvents. Nonetheless, the total wavelength range is not significantly different, and the absorption strength rises as the concentration does (Fig. 5, Tables 1-3).

Scanning electron microscopy (SEM) was used to further examine the structure and study the surface morphology of the LFC fluorescent complex. SEM is a high-resolution electron microscope that can examine the surface morphology and interactions with macromolecules' microstructure, making it a useful tool for detecting nanomaterials. As we can see from Fig. 6, the polymers are closely blended together to create a surface structure that is comparatively smooth by being layered layer by layer in the shape of scales.

Using transmission electron microscopy (TEM), the interior morphology of the LFC fluorescent complex was observed. The LFC fluorescent complex diffused outward in the acrylic resin system as branches (Fig. 7). The majority of fluorescent compounds are firmly packed together and entirely covered with acrylic resin. And to expand its surface area, spread out frequently, much like pine leaves do. This further suggests that this method's coating effect is more suited for the longer or ductile release applications of polymer nanomedicine.

PC3, HeLa and LO2 cells were chosen for cell proliferation assays so that the anti-proliferative properties of LFC on tumor cells could be observed. CCK-8 was used to measure the impact of LFC on PC3 and HeLa proliferation. LFC chemicals generally have a strong inhibitory effect on PC3 and HeLa cell growth. Good biological activity was demonstrated by the PC3 and HeLa treated with the drug, whose proliferation rates were 59.41% and 57.29%, respectively (Fig. 8 and Table 4). Its inhibiting impact also becomes highly evident as the concentration rises. However, for LO2 normal cells, the inhibition rate was only 69.25% and close to 70% at the highest drug concentration of 16 μg/mL. This indicates a lower toxic effect on normal cells.

Based on its stability and structure, the fluorescent complex's selectivity and biocompatibility in HeLa tumor cells were investigated using cell imaging. HeLa cell staining under a fluorescent microscope can be observed clearly with a laser confocal microscope. The bright field, DAPI, green channel, red channel, and merge imaging are displayed (Fig. 9). HeLa cells respond well to the LFC complex in terms of

selectivity and biocompatibility. It is evident that the blue visible specks are LFC complexes, which attach to and penetrate the tumor cells. In merge and overlay imaging, the staining effect of orange bright spots in tumor cells is vividly visible, despite being less evident in DAPI, green channel, and red channel. This suggests that the CBB-G-250 enhances and improves the selectivity and biocompatibility effects of *nido*-carborane small molecule medicines by driving them into targeted cells in the form of zwitterion.

4. Conclusion

The present investigation involved the combination of lipid-soluble carborane and water-soluble CBB-G-250 in the form of zwitterion following a strong alkali treatment. To achieve the desired effect and improve selectivity and biocompatibility to tumor cells, various types of acrylic resin were employed as coating carriers to form the form of water in oil. Applicability for this design is good. medication excipients were combined with amphoteric ion technology from the inside out to create a novel kind of fluorescent complex medication. The medication containing fluorescent complexes also inhibits the growth of malignant cells concurrently.

The LFC complexes have strong anticancer activity against PC-3 and Hela cells, with a 40% inhibition rate against tumor cells, according to CCK8 findings. In addition, it has a relatively low toxic effect on normal cells. The research and development of water-soluble *nido*-carborane fluorescent complexes can be facilitated by these pertinent facts, which can serve as a theoretical foundation.

Declaration of Competing Interest

The authors declare that they have no known competing financial interests or personal relationships that could have appeared to influence the work reported in this paper.

Acknowledgement

This study was supported financially by the scientific research foundation of Jiangsu University (Grant No. 17JDG002).

Appendix A. Supplementary data

Supplementary data to this article can be found online at <https://doi.org/10.1016/j.arabjc.2023.105511>.

References

- Bai, T., Zhao, K. Y., Lu, Z. J., Liu, X. F., Li, Z. Y., Zhu, D. W. and Zhang, L. H. et al., 2023. Simple fabrication of Cu²⁺-doped calcium alginate hydrogel filtration membrane with excellent anti-fouling and antibacterial properties. *Chinese Chem. Lett.* 32, 1051. <https://doi.org/10.1016/j.ccllet.2020.07.034>.
- Beerwerth, J., Böhmer, R., 2023. Low-temperature phase transitions and reorientational dynamics studied by 11B NMR in glassy crystal ortho-carborane. *J. Non-Crystalline Solids*: X. 18, 100180 <https://doi.org/10.1016/j.nocx.2023.100180>.
- Ecer, U., Yılmaz, S., Sahan, T., 2023. Synthesis, Characterization, and application of Ag-Doped Mercapto-Functionalized clay for decolorization of Coomassie brilliant Blue: Optimization using RSM. *Chem. Phys. Lett.* 825, 140610 <https://doi.org/10.1016/j.cplett.2023.140610>.
- Hasani, S., Mohamadnia, Z., Kazemi, F., et al., 2021. Preparation of microbeads grafted with poly(2-(acryloyloxy)ethyl] trimethylammonium chloride) cationic polyelectrolyte as recyclable and effective adsorbents for organic dyes. *React. Funct. Polym.* 169, 105087 <https://doi.org/10.1016/j.reactfunctpolym.2021.105087>.
- Hayakawa, M., Sunayama, N., Takagi, S.I., et al., 2023. Flattened 1D fragments of fullerene C60 that exhibit robustness toward multi-electron reduction. *Nat. Commun.* 14, 2741. <https://doi.org/10.1038/s41467-023-38300-3>.
- Hu, J., Wang, Y., Shao, T., et al., 2022. Simple and practical, highly sensitive and responsive recognition of cysteine: Design, synthesis and mechanism study of a novel curcumin fluorescent probe. *Arab. J. Chem.* 15, 104087 <https://doi.org/10.1016/j.arabjc.2022.104087>.
- Lee, D.Y., Lee, S., Lee, K.-G., et al., 2023. Synthetic colorants in capsule dietary supplements on the Korean market. *Food Addit. Contaminants: Part B*. 16, 93–101. <https://doi.org/10.1080/19393210.2022.2158495>.
- Lu, C., Yao, Z., Feng, J., et al., 2023. Oil-in-water strategy coating Curcumin-*nido*-Carborane fluorescent complex with acrylic resins for cell imaging. *Arab. J. Chem.* 16, 104876 <https://doi.org/10.1016/j.arabjc.2023.104876>.
- Mohamed, W.A.A., Abd El-Gawad, H.H., Handal, H.T., et al., 2023. Study of phototoxicity, remarkable photocatalytic activity, recycling process and energy consumption cost of TiO₂ quantum dots photocatalyst for photodegradation of Coomassie brilliant blue R dye. *Opt. Mater.* 137, 113607 <https://doi.org/10.1016/j.optmat.2023.113607>.
- Nagata, K., Ashikaga, R., Mori, W., et al., 2023. Analysis of the enzymatic degradation of lysozyme fibrils using a combination method of non-denaturing gel electrophoresis and double staining with Coomassie Brilliant Blue G-250 and R-250 dyes. *Anal Sci.* 39, 267–274. <https://doi.org/10.1007/s44211-022-00229-w>.
- Pariary, R., Dolui, S., Shome, G., et al., 2023. Coomassie brilliant blue G-250 acts as a potential chemical chaperone to stabilize therapeutic insulin. *Chem Commun (Camb)*. 59, 8095–8098. <https://doi.org/10.1039/d3cc01791e>.
- Phung, A.C., Fettingler, J.C., Power, P.P., 2023. Synthesis, Structure, and Spectroscopy of the Biscarboranyl Stannylenes (bc)Sn-THF and K₂[(bc)Sn]₂ (bc = 1,1'(ortho-Biscarborane)) and Dibiscarboranyl Ethene (bc)CH=CH(bc). *Organometallics* 42, 1649–1657. <https://doi.org/10.1021/acs.organomet.3c00190>.
- Sforzi, J., Lanfranco, A., Stefania, R., et al., 2023. A novel pH sensitive theranostic PLGA nanoparticle for boron neutron capture therapy in mesothelioma treatment. *Sci Rep.* 13, 620. <https://doi.org/10.1038/s41598-023-27625-0>.
- Shao, C., Lian, G., Jin, G., 2021. *Nido*-carborane encapsulated by BODIPY zwitterionic polymers: Synthesis, photophysical properties and cell imaging. *J. Saudi Chem. Soc.* 25, 101345 <https://doi.org/10.1016/j.jscs.2021.101345>.
- Shao, T., Wang, Y., Hu, K., et al., 2022. Nitrogen-boron eight-ring rigid cis/trans BODIPY-pyrimidine isomers for in vivo and in vitro fluorescence target recognition and evaluation of inhibitory activity. *Dyes Pigm.* 201, 110204 <https://doi.org/10.1016/j.dyepig.2022.110204>.
- Shi, Y., Guo, Z., Fu, Q., et al., 2023. Localized nuclear reaction breaks boron drug capsules loaded with immune adjuvants for cancer immunotherapy. *Nat Commun.* 14, 1884. <https://doi.org/10.1038/s41467-023-37253-x>.
- Valibeknejad, M., Abdoli, S.M., Alizadeh, R., Mihaila, S.M., Raoof, A., et al., 2023. Insights into transport in mucus barrier: Exploring particle penetration through the intestinal mucus layer. *J. Drug Deliv. Sci. Technol.* 86, 104752 <https://doi.org/10.1016/j.jddst.2023.104752>.
- Wang, S., Ding, Y., Zhang, L., Cheng, Y., Gu, J., Zhu, L., et al., 2023. Combination of colorimetry, inner filter effect-induced fluorometry and smartphone-based digital image analysis: A versatile and reliable strategy for multi-mode visualization of food dyes. *J. Hazard. Mater.* 445, 130563 <https://doi.org/10.1016/j.jhazmat.2022.130563>.
- Wang, Y., Xiao, F., Shao, T., et al., 2021. A multiple acetal chalcone-BODIPY-based fluorescence: synthesis, physical property, and biological studies. *Anal. Bioanal. Chem.* 413, 2529–2541. <https://doi.org/10.1007/s00216-021-03208-8>.
- Xu, C., Shao, T., Shao, S., et al., 2021. High activity, high selectivity and high biocompatibility BODIPY-pyrimidine derivatives for fluorescence target recognition and evaluation of inhibitory activity. *Bioorg Chem.* 114, 105121 <https://doi.org/10.1016/j.bioorg.2021.105121>.
- Zhang, R., Li, Y., Zhou, X., et al., 2023. Single-atomic platinum on fullerene C60 surfaces for accelerated alkaline hydrogen evolution. *Nat Commun.* 14, 2460. <https://doi.org/10.1038/s41467-023-38126-z>.
- Zhao, F., Hu, K., Shao, C., et al., 2021. Original boron cluster covalent with poly-zwitterionic BODIPYs for boron neutron capture therapy agent. *Polym. Test.* 100, 107269 <https://doi.org/10.1016/j.polymertesting.2021.107269>.
- Zimina, A.M., Kolpakova, T.V., Anufriev, S.A., et al., 2023. New 5-n-C4H9-C2B9-Carborane Ligand and Its Ruthenium Complexes. *Russ. J. Coord. Chem.* 49, 329–337. <https://doi.org/10.1134/S1070328423700604>.